Int. J. Heat Mass Transfer. Vol. 22, pp. 51–60
Pergamon Press Ltd. 1979. Printed in Great Britain

HEAT TRANSFER FROM A UNIFORM HEAT FLUX WEDGE IN AIR–WATER MIST FLOWS

T. AIHARA,† M. TAGA‡ and T. HARAGUCHI†

(*Received* 16 *December* 1977)

Abstract—Heat transfer from a wedge in air–water mist flow has been measured over a mass flow ratio M from 0 to 3×10^{-2}. Addition of small quantities of water-droplets to air stream enhanced two-phase heat-transfer coefficients $h_{(2)}$ from 2 to 14 times the corresponding single-phase ones. While the value of $h_{(2)}$ increases with increasing the wall temperature T_w at high mass flow ratios, it decreases with increasing T_w at low mass flow ratios, particularly in a dryout state. Generally $h_{(2)}$ increases with M and approach velocity. These tendencies are well explained by the present first-order theory.

NOMENCLATURE

a, distance between jet-exit and wedge;
b, half-width of jet-exit;
c_l, specific heat of water [kJ/kg K];
c_a, specific heat at constant pressure of humid air [kJ/kg* K, where * denotes dry air];
f_x, ratio of experimental value to theoretical one defined by equation (12);
G_e, mass evaporation rate of water film [kg/m² s];
G_p, mass flow rate of suspended droplets [kg/m² s];
h_x, local heat-transfer coefficient [W/m² K];
H, absolute humidity of humid air [kg/kg*];
l, length of wedge surface;
M, water-to-air mass flow ratio defined by equation (6);
Nu_x, local Nusselt number, $h_x x/\lambda_a$;
Pr_a, Prandtl number of humid air;
q, heat flux at wedge surface [W/m²];
r, latent heat of evaporation [kJ/kg];
Re_x, Reynolds number, $u_\infty x/\nu_a$;
T_∞, T'_∞, T_w, temperatures, dry-bulb and wet-bulb of jet, local wall respectively [K];
ΔT_{max}, $(T_w)_{max} - T_\infty$;
u_j, u_∞, velocities, at jet-exit and at the edge of boundary layer respectively [m/s];
v_∞, specific volume of humid air [m³/kg*];
x, y and x', y', Cartesian coordinates, see Fig. 2;
z, distance along the wedge apex measured from the centerline.

Greek symbols

λ_a, thermal conductivity of air [W/mK];
ν_a, kinematic viscosity of air [m²/s];
ϕ, apex angle of wedge [rad].

Subscripts

w, wedge surface;
(1), single-phase (air) flow;
(2), air–water mist flow;
∞, humid air of jet, unless mentioned specially.

Superscripts

$\bar{}$, average;
$\hat{}$, saturated humid air.

1. INTRODUCTION

FOR EFFECTIVE utilization of thermal energy, it is necessary that the temperature differences between heat-transferring fluids and solid surfaces and the power for transporting the fluid are as small as possible. Air–water mist cooling is one of the modern methods which meet these requirements. This method saves one from such special techniques to maintain the cooling film as in film- or ablation-cooling, because the liquid coolant is supplied to the heated surface by continuous impingement of water droplets laden in air stream.

Early studies of the heat transfer to air–water mist flow were experimentally made by Tanasawa [1] for fog quenching and by Takeyama [2] using heated wires. Thereafter Maezawa and Tsuchita [3], Heyt and Larsen [4], Simpson and Brolls [5, 6] and Bhatti and Savery [7] studied heat transfer from flat plates theoretically or experimentally. As for circular cylinders having active droplet-impingement, Hodgson *et al.* [8], Abe *et al.* [9], Kosky [10], and Mednick and Colver [11] carried out experiments; Goldstein *et al.* [12] and Hodgson and Sunderland [13] have made theoretical analyses neglecting gravity and water-film evaporation. Heat transfer from finned tubes in air–water mist flow was also measured by Simpson *et al.* [14]. Recently, Toda [15] made a review of mist cooling with boiling, in Japanese inclusive of his own study.

These results suggest that at low mass flow ratios, a remarkable heat-transfer enhancement is caused mainly by the evaporation of thin water films

†Institute of High Speed Mechanics, Tōhoku University, Sendai, Japan.
‡Mitsubishi Oil Co. Ltd., Mizushima, Kurashiki, Japan.

maintained effectively on heated surfaces. Accordingly, the authors have made an experiment on heat transfer from a wedge, having a simple geometry and an effective droplet-impingement, in the horizontal two-phase flows of air/water droplets (mean volume-surface diameter of 98–139 μm) at mass flow ratios from 0 to 3×10^{-2} and at wall temperatures below 69°C. Furthermore, a theoretical prediction is made on a simple model taking into account the water-film evaporation and compared with the experimental results.

2. EXPERIMENTAL APPARATUS AND PROCEDURE

2.1. *Air–water mist tunnel*

Figure 1 illustrates an outline of the wind tunnel and the spray system, whose details are described in [16]. First, room air was drawn into the inlet nozzle; after passing through a conic dust-filter, it suspended water mists in the spray chamber. Namely, after de-airing in a water tank, city water was pressurized by a three-throw plunger pump; then it was passed through a surge tank and an orifice meter; finally it was sprayed through ten hollow-cone spray nozzles which were arranged on a circle around the center-line of the chamber. A flat spray nozzle also was used for humidifying to saturate the carrier air. These nozzles were located sufficiently upstream so that drops larger than the desired ones might settle out of the mist in the low velocity spray-chamber, where turbulence also was attenuated. A heated test-wedge was installed horizontally in the potential core of a two-dimensional jet flow of air–water mists in the test chamber; the usual channel flow was not adopted to avoid a dropping from its ceiling, floodable floor, and blockage effect. In the case of no wedge, this potential core had the completely flat velocity profile. After heat-transferring, the exhaust air was demisted in an eliminator and drawn into a blower.

Since the water-to-air volume fraction is very small, average jet-exit velocities $\bar{u}_j$ were determined by the following equation:

$$\bar{u}_j = C_i(A_i v_j / A_j v_i)[2p_i v_i/(1+H_i)]^{1/2}, \qquad (1)$$

where A and C_i are the sectional area and discharge coefficient, calibrated in advance, of the inlet nozzle, p_i the static pressure defect at the nozzle measured by a Betz manometer, v the specific volume of humid air; and the subscripts i and j refer to the inlet- and jet-nozzles respectively.

2.2. *Test wedge*

The test surface was a stainless foil 30 μm thick and 240 mm wide which was fayed, by tensile forces acting on the end bars, along the midsurfaces of a 703 mm wide bakelite wedge body with a parallel trail as shown in Fig. 2. The foil was electrically heated by alternating current through electrodes; the Joule heat q_e was measured by the three-ammeters method. Surface temperatures T_w were measured with thirty-four 100 μm dia copper–constantan thermocouples soft-soldered to the backside of the foil; the errors due to the direct electric heating (max. 0.4°C throughout the whole experiment) were corrected by calibration. Vertical acrylic-resin plates were attached to both sides of the wedge body so as to prevent the water film escaping from there and to keep the flow two-dimensional.

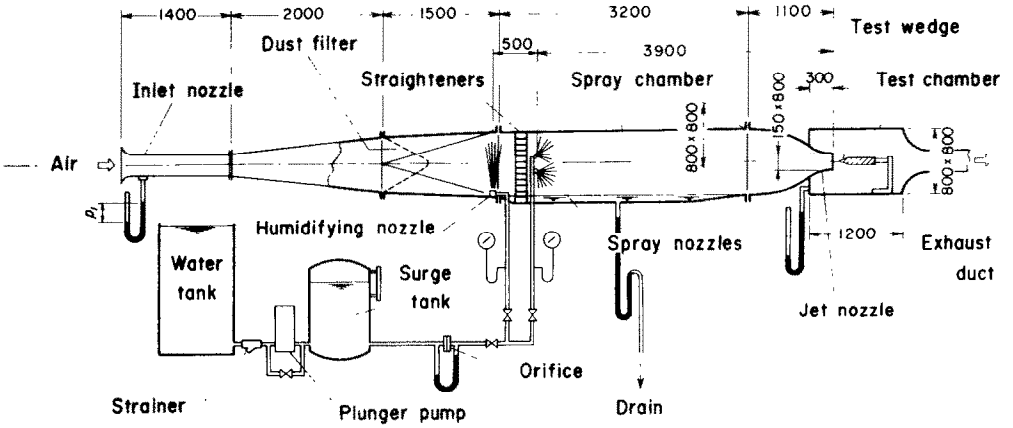

FIG. 1. Outline of wind tunnel and spray system (units of dimensions: mm).

The local heat-transfer coefficient h_x for the wedge surface, regardless of single- or two-phase, is defined as

$$h_x = q/(T_w - T_\infty), \qquad (2)$$

where T_∞ is the dry-bulb temperature of jet flow. The wall heat flux q is given as the sum of q_e and q_{cond}, the rate of heat conduction through the bakelite

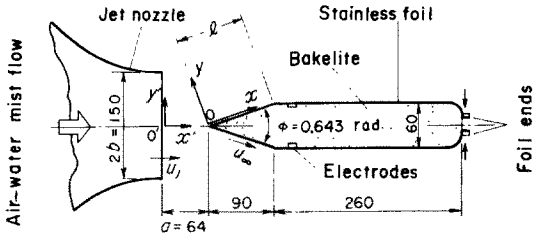

FIG. 2. Sectional view of test wedge and system of coordinates.

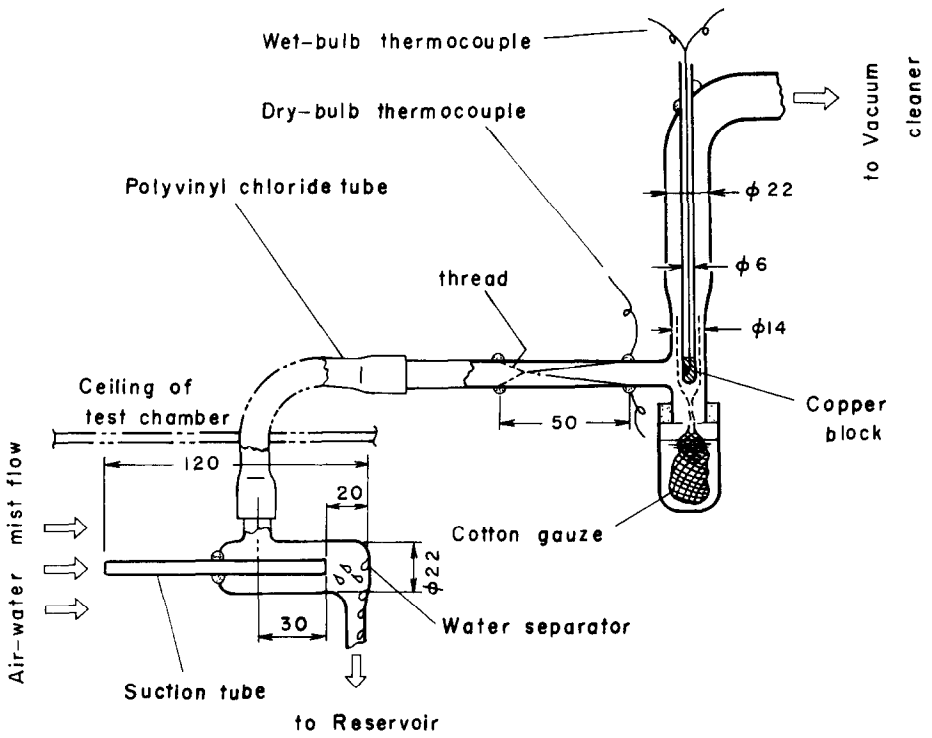

FIG. 3. Dry- and wet-bulb thermometers for air–water mists (not to scale).

body. The combined problems of external convection and internal conduction have been solved for a thin-wall wedge [17–19] and a wedge-shaped fin [20], but their thermal conditions differ from those of the present wedge body. Therefore in this study, q_{cond} was obtained by solving numerically the heat conduction equation with the measured values of T_w as the boundary condition; the values of q_{cond} were within 2% of q. After the heat-transfer experiment the stainless foil heater was removed from the wedge body and small holes for thermocouples were completely sealed with epoxiresin adhesive. Then, the static pressures were measured with 0.5 mm dia pressure holes drilled into its surface.

2.3. *Measurement of dry- and wet-bulb temperatures of humid air and droplet mass flow rate*

Gas-phase temperatures of the air–water mixture were measured by a device provided with 100 μm dia copper–constantan thermocouples as shown in Fig. 3. The mixture was sampled, at point 0′ (off-center: $z = +150$ mm) of Fig. 2, through the 7.5 mm I.D. and 9.4 mm O.D. glass suction tube inclining at an angle of about 65° with the jet flow. After separating the droplets, the air dry-bulb temperature was measured with a thermocouple stretched in a glass tube. Subsequently, the air wet-bulb temperature was measured by a thermocouple which was imbedded in a copper block covered with saturated gauze, when the average air velocity across the copper block was maintained so as to be 4 or 5 m/s by monitoring with an orifice flow meter. A preliminary experiment indicated that the effect of room temperature arisen from placing this device outside the test chamber was below 0.3°C.

The mass flow rate of suspended droplets, G_p, was measured by isokinetic sampling as shown in Fig. 4. The mixture sample was drawn into the 7.5 mm I.D. copper sampling tube, at the point of $x' = 0$, $y' = -10$ mm, and $z = -150$ mm, at the same air velocity as that of the potential core by monitoring with an

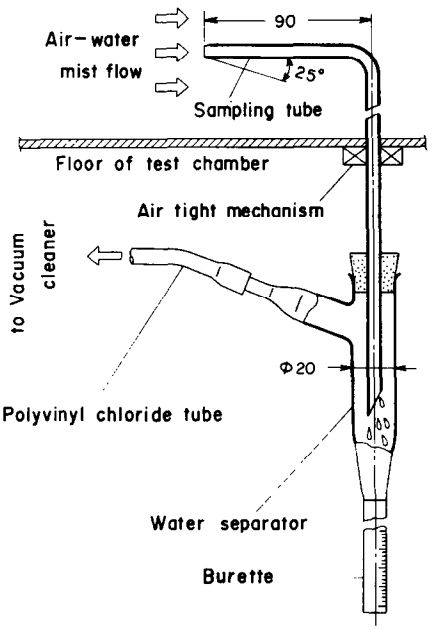

FIG. 4. Collection probe for measuring droplet flow rates (not to scale).

orifice flow meter. Then, the water droplets were separated from the mixture by inertia force in the separator made of glass and collected in a burette. The value of G_p was determined by dividing the mass collection rate, exclusive of starting period, by the sectional area of the sampling tube.

3. RESULTS AND DISCUSSION

3.1. *Single-phase heat transfer*

As a limiting case and a basis for future work, preliminary experiments were first performed in a single-phase (air alone) flow.

(i) *Velocity distribution.* Figure 5 shows typical distributions of the velocity at edge of boundary layer, u_∞, evaluated from the static pressures on the test wedge. In this figure, Okamoto *et al.*'s experimental data [22] on a wedge in channel flow (the ratio of wedge-length to channel-width $\cong 0.079$) are also plotted by interpolation from their data for the apex angles of $\pi/12$, $\pi/6$, $\pi/3$, $\pi/2$.

Now, we consider an ideal fluid flow around a finite wedge in a jet from a semi-infinite channel as a model similar to the present experimental condition. Its velocity distribution may be represented by the following equations on potential theory [21]:

$$u_\infty/\bar{u}_j = (\eta/s)^{\phi/2\pi}, \tag{3a}$$

$$\frac{x}{b} = \frac{s^{\phi/2\pi}}{\pi}\int_0^{\eta}\eta^{-\phi/2\pi}\left\{\frac{1}{s+\eta}+\frac{1}{s^{-1}+\eta} - \frac{2[\eta+\cos(2\pi\beta/\phi)]}{\eta^2+2\eta\cos(2\pi\beta/\phi)+1}\right\}d\eta, \tag{3b}$$

$$\frac{a}{b} = \frac{s^{\phi/2\pi}}{\pi}\,\text{v.p.}\int_0^{1}\xi^{-\phi/2\pi}\left\{\frac{1}{s-\xi}+\frac{1}{s^{-1}-\xi} - \frac{2[\xi-\cos(2\pi\beta/\phi)]}{\xi^2-2\xi\cos(2\pi\beta/\phi)+1}\right\}d\xi, \tag{3c}$$

where v.p. indicates the Cauchy principal value, η is the parameter obtained from equation (3b), and s and β are the parameters obtained from equation (3c) and equation (3b) with $x = l$ and the upper limit of integration = 1. In this connection, the velocity distribution on the wedge in channel flow can be calculated similarly by only putting $\beta = 1$ in these equations. The velocity distributions for both cases which are obtained by numerical integration of these equations, are also plotted in Fig. 5. It is seen by inspection of this figure that: the wedge in jet flow has the velocity distribution of $u_\infty \propto x^{\phi/(2\pi-\phi)}$, corresponding to infinite wedge flow, over the range of x/l more comprehensive than the wedge in usual channel flow; potential theory is in better agreement with the experiment on the former than on the latter. The measured velocities for both wedges increase more rapidly on approaching their trailing edges than the theory for ideal fluid; this tendency results from the fact that there exists a wake bubble in actual flow, in contrast to assuming infinite separation-streamlines in the theory.

(ii) *Heat-transfer coefficients.* The single-phase heat-transfer data for $\bar{u}_j$ of 5.5 and 7.4 m/s are plotted in Fig. 6 in terms of the local Nusselt number $Nu_{x(1)}$ and the Reynolds number Re_x, where u_∞ is estimated from a heavy dashed curve of Fig. 5 representing the measured velocities. The fluid properties are evaluated at the film temperature.

Levy's solution [23] for laminar wedge flows of $Pr = 0.7$ may be expressed as

$$Nu_{x(1)} = 0.424 Re_x^{0.5}, \tag{4}$$

where the value of coefficient, 0.424, is determined by interpolation from his numerical solutions; equation (4) is also plotted in Fig. 6. It is seen from the figure that the measured values tend to become higher than the theoretical ones with increasing the Reynolds number. Since Igarashi and Hirata's experimental results [24] for laminar wedge heat transfer (apex angle of $\pi/3$, $Re_x = 6\times10^3$–2×10^5) agree well with Levy's theory, the above tendency may be attributed to the rather high turbulence intensity in the potential core $[(\overline{u'^2})^{1/2}/\bar{u} = 1.6$–$1.7\%]$ due to the spray system existing upstream. It is well known [25] that in laminar flow with a pressure gradient, free-stream turbulence increases heat-transfer coefficients; however, the authors have never obtained information on this effect on wedge flows. Hence in the present report, the following empirical formula is derived after Lowery and Vachon's correlation for cylinders [26]:

$$Nu_{x(1)} = 0.424 Re_x^{0.5}(0.94 + 1.04\times10^{-3} Re_x^{0.5}). \tag{5}$$

This formula correlates the experimental data fairly well in the range of $2\times10^3 < Re_x < 6\times10^4$ as shown in Fig. 6.

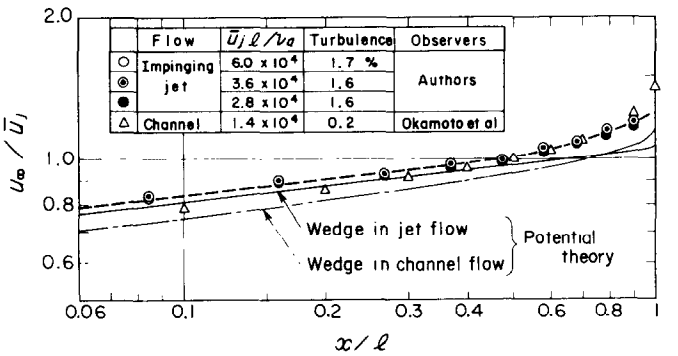

FIG. 5. Air velocity distributions on wedge surface of apex angle 0.643 rad.

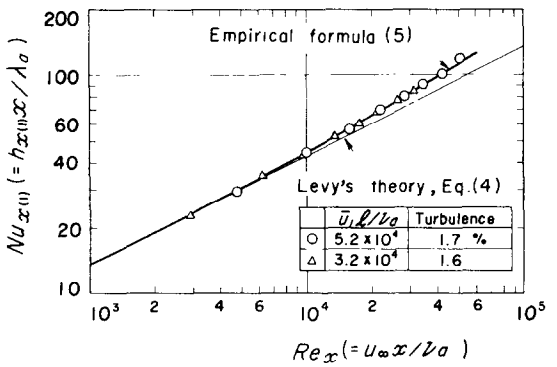

FIG. 6. Local heat-transfer coefficients for single-phase (air) flow $h_{x(1)}$.

3.2. *Two-phase heat transfer*

The experiment was carried out over ranges of the average air jet velocity $\bar{u}_j$ from 3.4 to 8.8 m/s, the wall heat flux q from 4.1×10^2 to 1.7×10^4 W/m^2, the relative humidity of air from 80 to 100% (the majority of data were above 88%), and the water to air mass flow ratio M, defined by equation (6), from 4.6×10^{-4} to 2.8×10^{-2}.

$$M=\frac{G_p v_\infty}{\bar{u}_j(1+H_\infty)}. \tag{6}$$

(i) *Suspended droplets and water film on the wedge surface.* Size distributions of the water droplets were measured at the point of $x=y=z=0$ by Nukiyama and Tanasawa's method [27]. Typical Rosin–Rammler distributions of them are shown in Fig. 7. The higher the relative humidity of room air and the mass flow ratio M, the larger is their size because of less droplet-evaporation in the spray

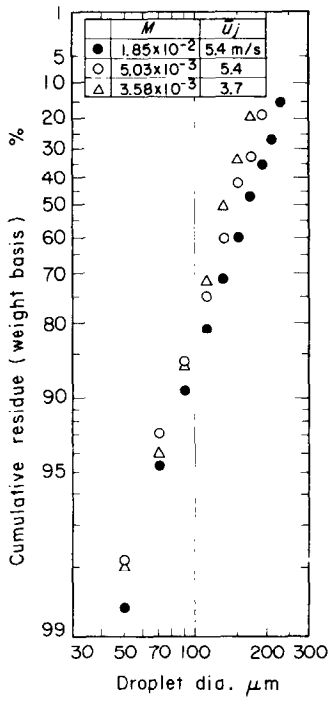

FIG. 7. Typical droplet-size distributions.

chamber; the jet velocity $\bar{u}_j$ shows essentially no effect within the experimental scatter of data. Throughout the whole experiment their mean volume-surface diameter was from 98 to 139 μm.

Droplet velocities were not measured in the present experiment. It should be, however, added that in our rough estimation the slip velocity of droplets is of the order of 2–17% of air velocity in the test section and the liquid mass flow rate, rather than droplet velocity, directly affects heat transfer coefficients. The vertical distribution of the liquid mass flow rate in mixture jet was within about +6 to −10%, though rather large in its lower part due to droplet settling.

Droplet trajectories were observed with the naked eye through one glass window on the side-walls of the test chamber, by superposing them and the straight lines which were drawn at regular intervals on a paper pinned against the outer surface of the other glass window. According to this observation, the droplets travel in nearly horizontal and straight paths and impinge the wedge surface. These straight droplet trajectories are to be expected from a consideration of the large "stopping distance" of 0.1 to 0.5 m in this experiment and from Goldstein *et al.*'s theoretical prediction for a circular cylinder [12].

It was found from observations with an 8 mm cinematography and with the naked eye that there is some difference in the behavior of the water film, produced by droplet impingement, between the upper and lower surfaces of the test wedge. Namely, in the large part of the upper surface, the water film flows downward to the leading edge of the wedge because gravitational force on the film is superior to the momentum influx due to droplets, the shear stress on the film due to gas component, and the like. It was, however, observed in the vicinity of the leading edge that surface tension stagnates the downward flow of water film and produces a semi-cylindrical swelling part as shown in Fig. 8. At low mass flow ratios, this swelling part is rather stable and has a width of about 8 mm. At high mass flow ratios, the following periodic flow motion was observed: the swelling part first grows up vibrating; as soon as its size exceeds a limit (e.g. its width $\bar{l}_s$ = 10–16 mm), the swelling part rapidly flows down from the upper surface to the lower one rounding the leading edge; and then all returns to the initial state. As air velocity is increased, its vibration becomes more violent, e.g. $\bar{l}_s\simeq$ 30–40 mm at $\bar{u}_j\simeq$ 8.8 m/s and $M\simeq10^{-2}$, and small ripples appear all over the water film. In some particular cases of high mass flow ratios, it was found that intermittently the crest of the swelling part is blown off and a re-entrainment occurs. Meanwhile on the lower surface, the water film flows smoothly downward, because the above-mentioned forces due to air–water mist flow act in the same direction as gravity.

In the case of low mass flow ratios and high heat fluxes, dryout of water film occurs successively from

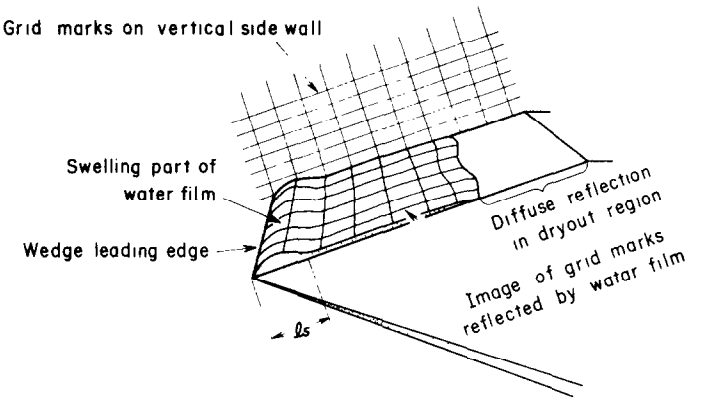

FIG. 8. Sketch of water film at a low air velocity ($\bar{u}_j \simeq 3.5$ m/s, $M = 4.7 \times 10^{-4}$).

the higher temperature surfaces where the mass evaporation rate of water film exceeds the mass impinging rate of droplets. It is possible to perceive the onset of dryout from a sudden rise in the wedge surface temperature or by macroscopic observation as in Fig. 8; however, in the present measurement either method gave nearly the same results.

(ii) *Heat-transfer coefficients.* The measured values of the time-average, two-phase heat-transfer coefficient $h_{x(2)}$ are shown in Fig. 9, where ΔT_{max} denotes the difference between the air dry-bulb temperature T_∞ and the average $(T_w)_{max}$ of the respective maximum temperatures of the upper and lower surfaces, and the curves of $h_{x(1)}$ for single-phase flow are evaluated from equation (5) for the same jet conditions as the two-phase runs. It may be seen that addition of small quantities of water-droplets to air stream enhances the two-phase heat-transfer coefficients from 2 to 14 times the corresponding single-phase ones. While at high mass flow ratios the local heat-transfer coefficient $h_{x(2)}$ increases with increasing ΔT_{max}, at low mass flow ratios it decreases with increasing ΔT_{max}. The latter tendency is particularly remarkable in the dryout regions which are represented in the figure by horned symbols such as ⊖⩚⩚. As a general tendency, the value of $h_{x(2)}$ increases as the water to air mass flow ratio M and the jet velocity, or approach velocity $\bar{u}_j$ are increased. The fact that the heat-transfer coefficient for upper surface has a maximum at $x/l \simeq 0.2$ or 0.3, seems to result from the violent vibration of swelling part which brings about a turbulent mixing and periodical thinning effects in the water film near the maximum point. The tendency for medium and low

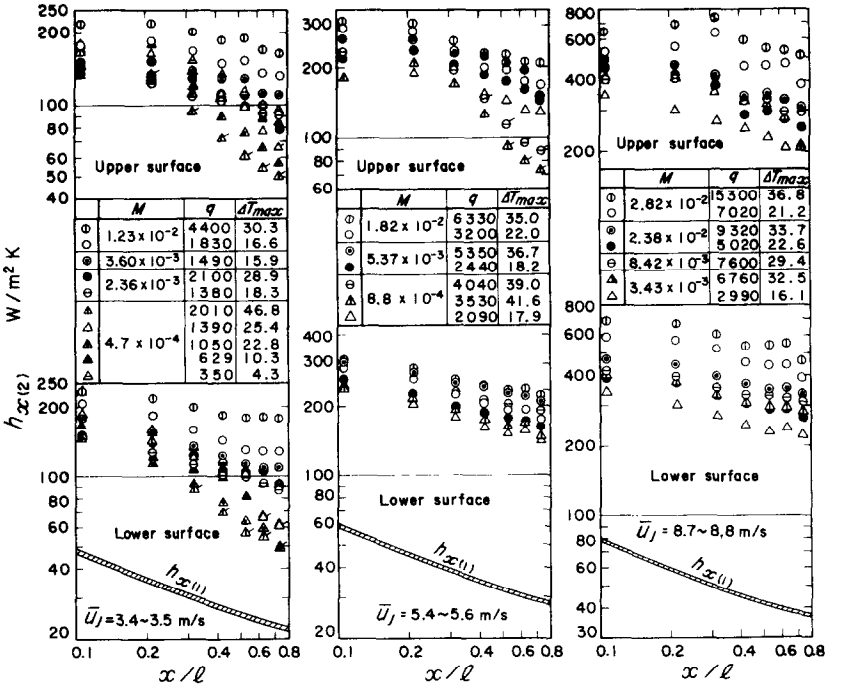

FIG. 9. Local heat-transfer coefficients for air–water mist flow $h_{x(2)}$ (q in W/m², T_{max} in °C; Symbols ⊙ and ● in right figure refer to $\bar{u}_j = 7.1$ m/s).

air velocities that at $x/l \simeq 0.1$ the heat-transfer coefficients for upper surface fall below the ones for lower surface, is caused by a flow stagnation, consequently a thickness increase of the water film near the leading edge.

4. FIRST ORDER THEORY AND COMPARISON WITH EXPERIMENT

4.1. *In fully wet regions*

The following assumptions are made for simplification:

(1) The presence of water droplets in the air stream does not affect the air flow around the wedge.

(2) The droplets are uniformly distributed in the jet flow; they travel with the mass velocity G_p and the same as the air wet-bulb temperature T'_∞ in straight paths parallel to the x'-axis.

(3) On impinging upon the wedge surface, the droplets immediately heat up to the bulk temperature of water film $\bar{T}_l$.

(4) The heat transfer from the film to the air follows the present empirical formula (5) for a dry wedge, and Lewis relation holds good between heat and mass transfer.

(5) No re-entrainment occurs.

With the foregoing assumptions, the time-average balances of mass and heat are as follows:

$$G_p \sin\frac{\phi}{2} = G_e + \frac{dW_l}{dx}, \tag{7}$$

$$q = h_{x(1)}(T_\delta - T_\infty) + G_e(r_\delta + c_l T_\delta) - G_p c_l T'_\infty \sin\frac{\phi}{2} + c_l \frac{d}{dx}(\bar{T}_l W_l), \tag{8}$$

where W_l and T_δ are the mass flow rate and surface temperature of the water film, r and c_l are the latent heat of vaporization and specific heat of water, and the subscript δ refers to the value at the temperature T_δ. Furthermore, the mass evaporation rate of water film G_e is approximated by

$$G_e \cong h_{x(1)}(\hat{H}_\delta - H_\infty)/c_a, \tag{9}$$

where c_a is the specific heat at constant pressure of humid air. All fluid properties in this chapter are evaluated at the film temperature and film humidity, unless mentioned specially.

Substitution of equations (7) and (9) into equation (8) and rearranging gives:

$$q = h_{x(1)}(T_\delta - T_\infty) \times \left\{1 + \frac{(\hat{H}_\delta - H_\infty)[r_\delta - c_l(\bar{T}_l - T_\delta)]}{(T_\delta - T_\infty)c_a}\right\} + G_p c_l(\bar{T}_l - T'_\infty)\sin\frac{\phi}{2} + c_l W_l \frac{d\bar{T}_l}{dx}. \tag{10}$$

Then the additional assumptions are introduced as follows:

(6) The temperature drop across the water film is negligible, i.e. $T_\delta \cong T_w$.

(7) The enthalpy transport by the water film also is negligible, i.e. $c_l W_l \, d\bar{T}_l/dx \cong 0$.

Substituting equation (2) in the LHS of the above equation,

$$h_{x(2)} \cong h_{x(1)}\left[1 + \frac{(\hat{H}_w - H_\infty)r_w}{(T_w - T_\infty)c_a}\right] + \frac{T_w - T'_\infty}{T_w - T_\infty} G_p c_l \sin\frac{\phi}{2}. \tag{11}$$

Now we consider the ratio of the measured heat-transfer coefficient of Fig. 9 to the predicted one according to equation (11), i.e.

$$f_x = [h_{x(2)}]_{exp}/[h_{x(2)}]_{th}, \tag{12}$$

and its average, $\bar{f}$, with respect to the wedge surface length l. Figure 10 is a plot of the values of $\bar{f}$ against the mass flow ratio M, exclusive of dryout data.

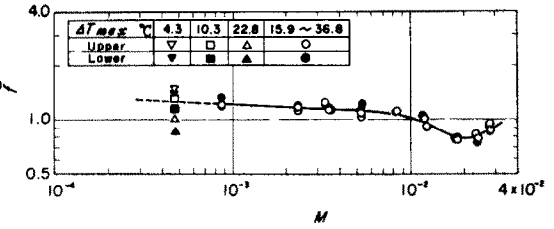

FIG. 10. Relation between the average ratio $\bar{f}$ of measured value to predicted one and the mass flow ratio M, exclusive of dryout data.

Excluding the case of extremely low mass flow ratio, the values of $\bar{f}$ almost depend upon M only. At relatively low mass flow ratios, $\bar{f}$ is greater than unity owing to assumption (4). However, with increasing the mass flow ratio, assumptions (3) and (6) become invalid due to the thickening water film and consequently $\bar{f}$ tends to decrease gradually; after reaching a minimum at $M \simeq 2 \times 10^{-2}$, $\bar{f}$ begins to increase again. This reincrease in $\bar{f}$ may be attributed to an increase in turbulence and to assumption (5). On the other hand, the smaller the mass flow ratio, the higher is the rate of droplets which diminish in size with evaporation in passing through the thermal boundary layer and flow away downstream without impinging on the wedge surface. This is the reason why at $M = 4.7 \times 10^{-4}$ the values of $\bar{f}$ decrease with increasing ΔT_{max}.

Figure 11 presents the distribution of local values f_x in a form normalized on the average values $\bar{f}$. Comparison of the average curves in this figure shows the following: As to the upper surface, although nearly uniform for low air velocities, the $f_x/\bar{f}$ has a maximum at $x/l \simeq 0.2$ for medium velocities and a wavy distribution with its maximum at $x/l \simeq 0.3$ for higher velocities; The abnormally small values at $x/l = 0.74$ seem to be caused by the droplet evaporation in the thermal boundary layer. In contrast to this, the distributions of $f_x/\bar{f}$ for the lower surface are nearly uniform independently of $\bar{u}_j$.

Next, we consider an enhancement factor of heat transfer defined as $h_{x(2)}/h_{x(1)}$. The single-phase heat-transfer coefficients of Fig. 6 can be also correlated simply as

$$h_{x(1)}x/\lambda_a \cong 0.29(u_\infty x/\nu_a)^{0.55}, \tag{13}$$

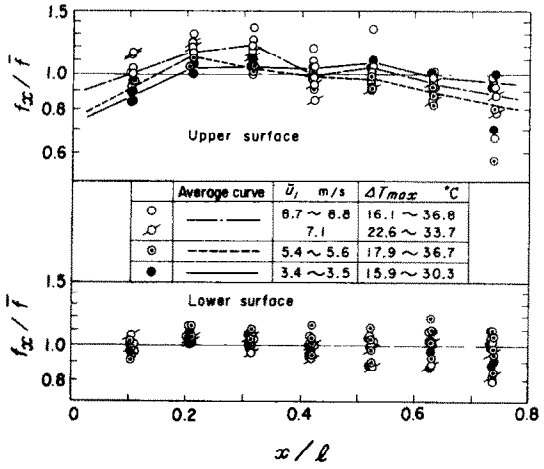

FIG. 11. Effect of jet velocity $\bar{u}_j$ upon the ratio f_x of measured value to predicted one, for $M \geqslant 8.8 \times 10^{-4}$ and exclusive of dryout data.

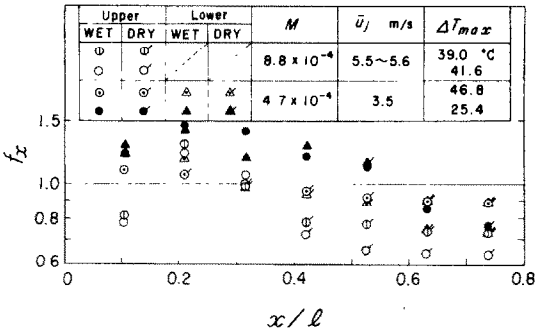

FIG. 12. Distributions of the ratio f_x of measured value to predicted one for the case of dryout onset.

in the experimental range. Therefore on the assumption of $T_\infty = T'_\infty$, i.e. relative humidity of 100%, the enhancement factor is obtained by substituting equations (6), (12), (13), into equation (11) as follows:

$$\left[\frac{h_{x(2)}}{h_{x(1)}}\right]_{exp} \cong f_x\left[1+\frac{(\hat{H}_w - H_\infty)r_w}{(T_w - T_\infty)c_a} + KM\bar{u}_j^{0.45}\right] \quad (14)$$

with

$$K = \frac{Pr_a}{0.29}\left(\frac{x}{\nu_a}\right)^{0.45}\left(\frac{\bar{u}_j}{u_\infty}\right)^{0.55}\left(\frac{c_l}{c_a}\right)\sin\frac{\phi}{2}. \quad (15)$$

While the value of K is nearly constant for a given position x, the second term on the RHS of equation (14) increases with the wall temperature. Hence excluding the case of low mass flow ratio, the enhancement factor increases obviously with $(T_w - T_\infty)$, M, and $\bar{u}_j$, even if the relation of Fig. 10 is considered. This supports the general tendency of $h_{x(2)}$ described in Section 3.2.(ii).

4.2. *In dryout regions*

Since in this case the droplets impinging on the wedge surface evaporate out there, the time-average balances of mass and heat are approximated as:

$$G_p \sin\frac{\phi}{2} \cong G_e, \quad (16)$$

$$q \cong h_{x(1)}(T_w - T_\infty) + G_e(r_w + c_l T_w) - G_p c_l T'_\infty \sin\frac{\phi}{2}. \quad (17)$$

Substituting equations (2) and (16) into equation (17),

$$h_{x(2)} \cong h_{x(1)} + \frac{r_w + c_l(T_w - T'_\infty)}{T_w - T_\infty} G_p \sin\frac{\phi}{2}. \quad (18)$$

The respective local heat-transfer coefficients, $[h_{x(2)}]_{th}$, for the dryout and wet surfaces are estimated from equations (18) and (11); and a comparison with the experimental values, $[h_{x(2)}]_{exp}$, is shown in Fig. 12 in terms of f_x. The experimental data for the dryout surface are mostly lower than the corresponding theoretical values, owing to the droplet evaporation in passing through the boundary layer.

The enhancement factor for dryout surface can be derived from equations (6), (13) and (18) on the assumption of $T_\infty = T'_\infty$, in the same manner as in the foregoing Section:

$$\frac{h_{x(2)}}{h_{x(1)}} \simeq 1 + \left[1 + \frac{r_w}{(T_w - T_\infty)c_l}\right] KM\bar{u}_j^{0.45}. \quad (19)$$

It is seen from this equation that at such low mass flow ratios as to cause the dryout, the enhancement factor decreases with increasing $(T_w - T_\infty)$ as described in Section 3.2.(ii).

5. CONCLUSIONS

The results obtained are summarized as follows:

(1) The measured values of the velocity at the edge of boundary layer for single-phase (air alone) runs, agree fairly well with potential theory for an ideal fluid flow around a finite wedge in a jet. The measured heat-transfer coefficients in a single-phase flow tend to become slightly greater than Levy's laminar theory with increasing the Reynolds number, owing to free-stream turbulence of about 1.7%; an empirical formula, holding good over the range of $2 \times 10^3 < Re_x < 6 \times 10^4$, is derived by taking account of this tendency.

(2) The addition of water-droplets to air stream at such small mass flow ratios as 5×10^{-4}–3×10^{-2}, enhances the two-phase heat-transfer coefficients from 2 to 14 times the corresponding single-phase ones.

(3) There is some difference between the upper and lower surfaces of a wedge in the behavior of the water film produced by droplet impingement. Particularly on the upper surface, its heat-transfer coefficient has a maximum at $x \simeq 20$–30 mm, owing to the violent oscillation of the swelling part of water film in the vicinity of the leading edge of wedge; and the dryout of water film also is more liable to occur on the upper surface. However,

excluding these points, there is little difference between them in the heat-transfer data correlated as in Chapter 4.

(4) As a general tendency, the two-phase local heat-transfer coefficient $h_{x(2)}$ increases with increasing the mass flow ratio and approach velocity. While at high mass flow ratios the value of $h_{x(2)}$ increases as the wedge surface temperature T_w is increased, at low mass flow ratios (particularly in dryout regions) it decreases as T_w is increased.

(5) The above-mentioned tendencies are theoretically corroborated by considering the time-average balances of mass and heat on an approximate model taking account of the evaporation and dryout of water-film. From the relatively good agreement between the first order theory and the experiment, it is considered that the droplet evaporation in thermal boundary layer and the effect of water film on gas-phase boundary layer are of second order.

Acknowledgements—The authors wish to express their thanks to several staff members of the Institute of High Speed Mechanics: to Professor T. Yuge for giving an opportunity for the present study and his help, to Professor H. Itoh for lending them a DISA hot-wire anemometer, to Dr. A. Sasago for his assistance in computations, to Mr. S. Endoh for his assistance in making this experiment, and to Miss Y. Kumagai for her assistance in preparing the manuscript. They also wish to express their gratitude to Professor K. Sekoguchi of Kyushu University and to Professor N. Nagai of Tōhoku University for giving them references [5, 6, 14] and references to atomization respectively.

The research has been carried out partly with the Grants-in-aid for Scientific Research and for Special Research Equipment of the Ministry of Education of Japan. It is a pleasure to express our gratitude to them here.

REFERENCES

1. Y. Tanasawa, Y. Miyasaka, M. Umehara and H. Kamata, Study of fog quenching (Part 1), *J. Japan. Soc. Mech. Engrs* **50**, 9–14 (1947).
2. T. Takeyama, Heat transfer from electrically heated horizontal wire to sprayed jet, *Trans. Japan. Soc. Mech. Engrs* **27**, 1319–1326 (1961).
3. S. Maezawa and A. Tsuchita, Mass and heat transfer in flow of gas with liquid-droplet suspension (1st report, laminar boundary layer on a flat plate), Preprints *7th Heat Transfer Symposium of Japan*, pp. 145–148 (1970).
4. J. W. Heyt and P. S. Larsen, Heat transfer to binary mist flow, *Int. J. Heat Mass Transfer* **14**, 1395–1405 (1971).
5. H. C. Simpson and E. K. Brolls, Heat transfer from a thick flat plate to an air–water mist in turbulent flow over the plate, in *Proceedings of the Symposium on Multi-Phase Flow Systems*, Inst. Chem. Engrs Symp. Ser. No. 38, Paper No. H2, pp. 1–23 (1974).
6. H. C. Simpson and E. K. Brolls, Droplet deposition on a flat plate from an air–water mist in turbulent flow over the plate, in *Proceedings of the Symposium on Multi-Phase Flow Systems*, Inst. Chem. Engrs Symp. Ser. No. 38, Paper No. A3, pp. 1–25 (1974).
7. M. S. Bhatti and C. W. Savery, Augmentation of heat transfer in a laminar external gas boundary layer by the vaporization of suspended droplets, *J. Heat Transfer* **97**, 179–184 (1975).
8. J. W. Hodgson, R. T. Saterbak and J. E. Sunderland, An experimental investigation of heat transfer from a spray cooled isothermal cylinder, *J. Heat Transfer* **90**, 457–463 (1968).
9. A. Abe, M. Ōuchi, S. Simizu and T. Takeyama, Forced convection heat transfer from horizontal cylinder to sprayed jet, Preprints *4th Heat Transfer Symposium of Japan*, pp. 49–52 (1967).
10. P. G. Kosky, Heat transfer to saturated mist flowing normally to a heated cylinder, *Int. J. Heat Mass Transfer* **19**, 539–543 (1976).
11. R. L. Mednick and C. P. Colver, Heat transfer from a cylinder in an air–water spray flow stream, *A.I.Ch.E. Jl* **15**, 357–362 (1969).
12. M. E. Goldstein, Wen-Jei Yang and J. A. Clark, Momentum and heat transfer in laminar flow of gas with liquid-droplet suspension over a circular cylinder, *J. Heat Transfer* **89**, 185–194 (1967).
13. J. W. Hodgson and J. E. Sunderland, Heat transfer from a spray-cooled isothermal cylinder, *I/EC Fundamentals* 7, 567–572 (1968).
14. H. C. Simpson, G. C. Beggs and G. N. Sen, Heat transfer from extended surface tubes to an air–water mist, in *Proceedings of the Symposium on Multi-Phase Flow Systems*, Inst. Chem. Engrs Ser. No. 38, Paper No. H3, pp. 1–22 (1974).
15. S. Toda, Mist cooling heat transfer, in *Dennetsu Kōgaku no Shinten (Progress in Heat Transfer)*, Vol. 3, pp. 211–330. Yokendoh, Tokyo (1974).
16. T. Aihara and M. Taga, Structure and performance of a wind tunnel for air–water mist flows, *Mem. Inst. High Speed Mech., Tōhoku Univ.* **38**, 23–34 (1976).
17. B. T. Chao and L. S. Cheema, Forced convection in wedge flow with non-isothermal surfaces, *Int. J. Heat Mass Transfer* **14**, 1363–1375 (1971).
18. M. Sakakibara, K. Endoh, S. Mori and A. Tanimoto, Effect of conduction in wall on convective heat transfer with laminar boundary layer from a flat plate inclined to main flow—wedge flow, *Kagaku Kogaku, Soc. Chem. Engrs Japan* **38**, 612–614 (1974).
19. A. V. Luikov, T. L. Perelman, R. S. Levitin, L. B. Gdalevich and B. M. Khusid, Characteristics of external conjugated heat transfer in fluid flows around bodies, in *Proceedings of the International Heat Transfer Conference*, Tokyo, II, Paper No. FC 8.1, pp. 295–299 (1974).
20. U. Olsson, Laminar flow heat transfer from wedge-shaped bodies with limited heat conductivity, *Int. J. Heat Mass Transfer* **16**, 329–336 (1973).
21. M. I. Gurevich, *Theory of Jets in Ideal Fluids*. Academic Press, New York (1965).
22. T. Okamoto, K. Ōtsuka and M. Yagita, Experimental investigation on the wake of a wedge, Preprints Japan. Soc. Mech. Engrs, No. 730, pp. 59–62 (1973).
23. S. Levy, Heat transfer to constant-property laminar boundary-layer flows with power-function free-stream velocity and wall-temperature, *J. Aeronaut. Sci.* **5**, 341–348 (1952).
24. T. Igarashi and M. Hirata, Heat transfer in wedge flow, Preprints Japan. Soc. Mech. Engrs, No. 720, pp. 17–20 (1972).
25. J. Kestin, P. F. Maeder and H. E. Wang, Influence of turbulence on the transfer of heat from plates with and without a pressure gradient, *Int. J. Heat Mass Transfer* **3**, 133–154 (1961).
26. G. W. Lowery and R. I. Vachon, The effect of turbulence on heat transfer from heated cylinders, *Int. J. Heat Mass Transfer* **18**, 1229–1242 (1975).
27. S. Nukiyama and Y. Tanasawa, Experiment on atomization of liquid by means of air stream (Part 1), *Trans. Japan Soc. Mech. Engrs* **4**, 128–135 (1938).

TRANSFERT THERMIQUE POUR UN DIEDRE AVEC FLUX UNIFORME DANS UN ECOULEMENT D'AIR ET D'EAU EN BROUILLARD

Résumé—On mesure le transfert thermique pour un dièdre plaçé dans l'écoulement d'un brouillard d'eau et d'air, pour un rapport de débits massique M allant de zéro à 3×10^{-2}. L'addition d'une petite quantité de gouttes d'eau à l'air fait que le coefficient de transfert $h_{(2)}$ en écoulement diphasique est de 2 à 14 fois celui correspondant à l'écoulement monophasique. Alors que la valeur de $h_{(2)}$ augmente avec la température pariétale T_w pour des rapports massiques élevés, elle diminue lorsque T_w croît pour les faibles valeurs du rapport massique, particulièrement dans l'état d'assèchement. Ces tendances sont explicables par la théorie au premier ordre donnée ici.

WÄRMEÜBERGANG VON EINEM KEIL BEI KONSTANTEM WÄRMESTROM IN STRÖMUNGEN VON LUFT-WASSER-NEBEL

Zusammenfassung—Es wurde der Wärmeübergang von einem Keil in einem Strom aus Luft-Wasser-Nebel in Abhängigkeit vom Massenstromverhältnis M im Bereich von 0 bis 3×10^{-2} gemessen. Die Zugabe kleinerer Mengen von Wassertropfen in den Luftstrom erhöhte die 2-Phasen-Wärmeübertragungskoeffizienten $h_{(2)}$ vom 2-fachen bis zum 14-fachen Wert der entsprechenden Wärmeübergangskoeffizienten bei einphasigen Medien. Während der Wert von $h_{(2)}$ bei hohen Massenströmen mit steigenden Wandtemperaturen T_w zunimmt, wird er bei kleinen Massenstromverhältnissen mit steigendem T_w kleiner, besonders im Zustand des Austrocknens. Meistens wird $h_{(2)}$ mit wachsendem M und zunehmender Anfangsgeschwindigkeit größer. Diese Tendenzen werden mit der vorliegenden Theorie erster Ordnung gut erklärt.

ТЕПЛООБМЕН МЕЖДУ РАВНОМЕРНО НАГРЕТЫМ КЛИНОМ И ПОТОКОМ НАСЫЩЕННОГО ВЛАГОЙ ВОЗДУХА

Аннотация — Исследуется теплообмен между клином и потоком насыщенного влагой воздуха в диапазоне отношений массовых потоков M от 0 до 3×10^{-2}. Введение в поток воздуха небольшого количества водяных капель увеличивает коэффициент теплообмена двухфазного потока $h_{(2)}$ в 2–14 раз по сравнению с однофазными потоками. В то время как значение $h_{(2)}$ увеличивается с ростом температуры стенки T_w при больших отношениях массовых потоков, оно уменьшается с ростом T_w при малых значениях отношений, особенно в точке высыхания. Вообще, коэффициент $h_{(2)}$ возрастает с ростом M и скорости течения. Наблюдаемые закономерности хорошо объясняются с помощью предложенной в работе теории.